Bimodal first-passage times on a 2D $N \times N$ lattice with biased/lazy random walks

Summary and Key Figures

- **Candidate A** (periodic boundary + global bias): the FPT is bimodal under a unified criterion; fast/slow channels arise from an "against-drift shortcut" and a "with-drift wrap-around" path; AW inversion matches exact recursion on $t \le t_{\max}^{\mathrm{AW}}$ and MC overlays (Fig. 7, 9).
- **Candidate B** (edge corridor + mixed boundary): auto-tuning yields $g_x = -0.25$, $g_y = 0.40$, $\delta = 0.70$ and allows an x-periodic boundary to create a slow wrap-around channel, lifting the fast weight into a visible range; bimodality is clear in the peak–valley zoom (Fig. 15).
- **Candidate C** (door + sticky + wrap-around): bimodality already appears at $n_{\mathrm{bias}} = 0$, i.e., the minimum local bias count is zero (Fig. 28).
- Numerical comparison: AW inversion (frequency domain) and exact recursion (time domain) reach $\mathcal{O}(10^{-12})$ L^1 error for $t \le t_{\max}^{\mathrm{AW}}$ (Table 3 and error metrics).

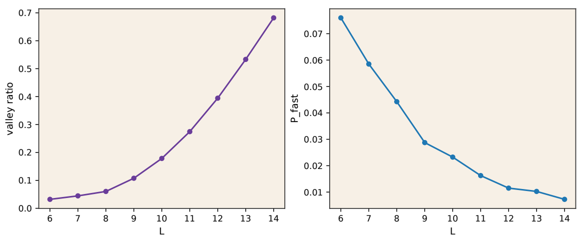

(a) Candidate B scan

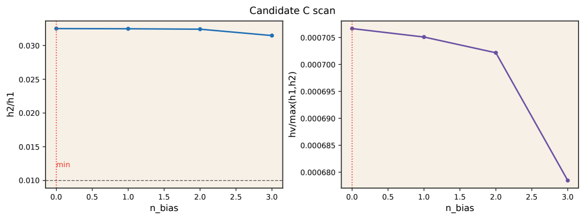

(b) Candidate C scan

Figure 1: Scan results for minimal corridor length and minimal local bias sites (B and C).

Parameter Table

case	N	q	g_x	g_y	boundary	(start, target)
A	60	0.8	+0.6	0	x periodic, y reflecting	(10,30)→(12,30)
B	60	0.8	-0.25	+0.40	x periodic, y reflecting	(50,60)→(42,60)
C	60	0.8	+0.5	0	x periodic, y reflecting	(10,30)→(50,30)

Table 1: Core parameters for the three candidates. Candidate B uses an edge corridor with auto-tuned (g_x, g_y); Candidate C uses door + sticky and preserves a wrap-around channel.

1 Model Definition and Coordinate Convention

The state space is $\{1,\ldots,N\} \times \{1,\ldots,N\}$. The walker is at (x,y) and the target (x_t,y_t) is absorbing. One-step transition probabilities are

$$p_{\text{left}} = \frac{q}{4}(1+g_x), \quad p_{\text{right}} = \frac{q}{4}(1-g_x), \tag{1}$$

$$p_{\text{down}} = \frac{q}{4}(1+g_y), \quad p_{\text{up}} = \frac{q}{4}(1-g_y), \tag{2}$$

$$p_{\text{stay}} = 1-q. \tag{3}$$

We adopt the convention "y increases downward", so $g_y > 0$ means downward drift. Boundaries are reflecting, periodic, or mixed (x periodic, y reflecting). From Eq.(1), $g_x > 0$ increases $p_{\text{left}} = \frac{q}{4}(1+g_x)$ and decreases $p_{\text{right}} = \frac{q}{4}(1-g_x)$, so we define $g_x > 0$ as a **leftward** global bias ($g_x < 0$ is rightward).

Local heterogeneities (combinations).

- local bias (arrow): multiply p_{stay} by $(1-\delta)$ and add $\Delta = \delta p_{\text{stay}}$ to the arrow direction; other directions stay unchanged.
- sticky site: scale the move rate to $q_{\text{site}} = \text{factor} \cdot q$ (default 0.2); p_{stay} increases accordingly.
- barrier: a reflecting edge adds its probability back to stay; a door passes with p_{pass} and reflects with $1 - p_{\text{pass}}$.

2 How to Read the Figures

Fig. 2 gives the unified symbol legend: red squares are starts, blue diamonds are targets; thick solid lines are reflecting walls, dashed lines are doors (labeled by p_{pass}), translucent shading is sticky regions; red arrows are local bias sites; large arrows outside the grid indicate the global drift and (g_x, g_y). For readability, environment schematics, $P(n,t)$ slices, multiscale FPT plots, and channel decompositions are shown as separate figures; Candidate B adds a peak–valley zoom to emphasize the early peak and valley.

Figure 2: Symbol legend.

3 Analytical derivation: from defect-free propagator to time-domain FPT

This section provides a unified derivation chain: *defect-free propagator* $\to$ *defect propagator* $\to$ *FPT generating function* $\to$ *AW inversion*. All three candidates fit this framework.

3.1 Matrix form and generating function

Let A be the transition matrix for the non-absorbing system, with $A_{v,u} = \Pr(u \to v)$ so columns sum to 1 and $\mathbf{p}_{t+1} = A\mathbf{p}_t$. The propagator satisfies

$$P_{n_0}(n,t) = \mathbf{e}_n^\top A^t \mathbf{e}_{n_0}, \qquad \tilde{\mathbf{P}}(z) = \sum_{t\geq 0} A^t z^t = (I - zA)^{-1}, \tag{4}$$

so

$$\tilde{P}_{n0}(n,z) = \mathbf{e}_n^\top (I - zA)^{-1}\mathbf{e}_{n0}. \tag{5}$$

We now give the spectral form of A and the defect update formula to obtain $\tilde{P}$ for any configuration.

3.2 Spectral decomposition of the defect-free propagator

Write the 2D update as the sum of two 1D operators (along x and y). Let $\{\lambda_k^{(\gamma)}, h_k^{(\gamma)}\}$ be eigenpairs of the 1D step matrix, where $\gamma \in \{\text{periodic}, \text{reflecting}\}$ denotes boundary type. Define

$$s_k^{(\gamma)} = q\left(\lambda_k^{(\gamma)} - 1\right), \qquad \Lambda_{k_1,k_2} = 1 + \frac{s_{k_1}^{(\gamma_x)} + s_{k_2}^{(\gamma_y)}}{2}. \tag{6}$$

Then the 2D defect-free propagator (Eq.(33) in PRE 102, 062124) is

$$P_{n_0}^{(\gamma)}(n,t) = \sum_{k_1}\sum_{k_2} h_{k_1}^{(\gamma_x)}(x,x_0)\, h_{k_2}^{(\gamma_y)}(y,y_0)\, \Lambda_{k_1,k_2}^t. \tag{7}$$

The z-transform is

$$\tilde{P}_{n_0}^{(\gamma)}(n,z) = \sum_{k_1}\sum_{k_2} \frac{h_{k_1}^{(\gamma_x)}(x,x_0)\, h_{k_2}^{(\gamma_y)}(y,y_0)}{1 - z\Lambda_{k_1,k_2}}. \tag{8}$$

Periodic boundary (periodic)

$$\theta_k = \frac{2\pi k}{N}, \quad \lambda_k^{(\text{per})} = \frac{1+g}{2}e^{-i\theta_k} + \frac{1-g}{2}e^{i\theta_k}, \quad h_k^{(\text{per})}(x,x_0) = \frac{1}{N}e^{i\theta_k(x-x_0)}. \tag{9}$$

Reflecting boundary (reflecting) Let $p_\ell = (1+g)/2$, $p_r = (1-g)/2$, $\rho = p_r/p_\ell$. A similarity transform symmetrizes the 1D operator, giving

$$\lambda_0^{(\text{ref})} = 1, \quad \lambda_k^{(\text{ref})} = 2\sqrt{p_\ell p_r}\cos\frac{k\pi}{N}\ (k \geq 1), \quad h_k^{(\text{ref})}(x,x_0) = u_k(x)u_k(x_0)\sqrt{\frac{\pi_x}{\pi_{x_0}}}, \tag{10}$$

where $\pi_x \propto \rho^x$ is the stationary distribution and u_k are orthogonal cosine modes (matching PRE Eq.(22)–(23)).

3.3 Determinant formula for defect propagator

Write the defect as a matrix perturbation $\underline{X} = \underline{B} - \underline{A}$. For each directed edge $(u_i \to v_i)$, define

$$\eta_{u_i,v_i} = X_{v_i,u_i} = B_{v_i,u_i} - A_{v_i,u_i}. \tag{11}$$

Define the difference propagator

$$\tilde{P}^e_{\langle u-v\rangle}(n,z) = \tilde{P}^e_u(n,z) - \tilde{P}^e_v(n,z). \tag{12}$$

Then the inert-heterogeneity formula (2311.00464v2) gives

$$\tilde{P}_{n_0}(n,z) = \tilde{P}^e_{n_0}(n,z) - 1 + \frac{\det[H(n,n_0;z)]}{\det[H(z)]}, \tag{13}$$

with

$$H_{ij}(z) = -\frac{\delta_{ij}}{z} + \eta_{u_j,v_j}\,\tilde{P}^e_{\langle u_j - v_j\rangle}(u_i,z) - \eta_{v_j,u_j}\,\tilde{P}^e_{\langle u_j - v_j\rangle}(v_i,z), \tag{14}$$

$$H(n,n_0;z)_{ij} = H_{ij}(z) - \tilde{P}^e_{\langle u_j - v_j\rangle}(n,z)\left[\eta_{u_i,v_i}\tilde{P}^e_{n_0}(u_i,z) - \eta_{v_i,u_i}\tilde{P}^e_{n_0}(v_i,z)\right]. \tag{15}$$

In numerical implementations, we solve the equivalent linear system for stability (by Cramer equivalence). The linear-algebra form reads

$$b_j(n,z) = \tilde{P}^e_{u_j}(n,z) - \tilde{P}^e_{v_j}(n,z), \tag{16}$$

$$a_i(n_0,z) = \eta_{u_i,v_i}\tilde{P}^e_{n_0}(u_i,z) - \eta_{v_i,u_i}\tilde{P}^e_{n_0}(v_i,z), \tag{17}$$

$$H_{ij}(z) = -\frac{\delta_{ij}}{z} + \eta_{u_j,v_j}\, b_j(u_i,z) - \eta_{v_j,u_j}\, b_j(v_i,z), \tag{18}$$

so that

$$\tilde{P}_{n_0}(n,z) = \tilde{P}^e_{n_0}(n,z) - \mathbf{b}(n,z)^\top H(z)^{-1}\mathbf{a}(n_0,z). \tag{19}$$

Defect mapping (used in B/C)

- local bias: reduce the self-loop and add probability to the arrow direction, equivalent to $(u \to v)$ with $\eta_{u,v} = +\Delta$, plus a compensation term for $(u \to u)$ to keep column sums at 1.
- door/permeable barrier: crossing the door multiplies by p_{pass}; both $(u \to v)$ and $(v \to u)$ have $\eta_{u,v} = (p_{\text{pass}} - 1)P^{\text{base}}_{u\to v}$.
- sticky: multiply all outgoing edges by α; each outgoing edge $(u \to n)$ has $\eta_{u,n} = (\alpha-1)P^{\text{base}}_{u\to n}$, with a compensation term added to $(u \to u)$ to keep column sums at 1.

feature	rule (example $u \to v$)	corresponding $\lambda_{u,v}$
local bias	$p_{u\to v} = p^0_{u\to v} + \Delta$	$-\Delta/p^0_{u\to v}$
sticky	$p_{u\to v} = \alpha p^0_{u\to v}$	$1-\alpha$
barrier	$p_{u\to v} = 0$	1
door	$p_{u\to v} = p_{\text{pass}}p^0_{u\to v}$	$1 - p_{\text{pass}}$

Table 2: Mapping from features to λ ($\eta_{u,v} = -\lambda_{u,v}p^0_{u\to v}$).

3.4 FPT generating function and AW inversion

Consider the master equation with an absorbing state:

$$\mathbf{p}_{t+1} = P\,\mathbf{p}_t, \qquad \mathbf{p}_0 = \mathbf{e}_{n_0}, \tag{20}$$

with z-transform $\tilde{\mathbf{p}}(z) = \sum_{t\geq 0}\mathbf{p}_t z^t$ giving

$$\tilde{\mathbf{p}}(z) = (I - zP)^{-1}\mathbf{p}_0. \tag{21}$$

Let the cumulative arrival probability be $F(t) = \mathbf{e}_{n_t}^\top \mathbf{p}_t$, then

$$\tilde{F}(z) = \mathbf{e}_{n_t}^\top (I - zP)^{-1}\mathbf{p}_0. \tag{22}$$

With $f(t) = F(t) - F(t-1)$ (take $F(-1) = 0$), the PMF generating function is

$$\tilde{f}(z) = (1-z)\tilde{F}(z) = (1-z)\,\mathbf{e}_{n_t}^\top (I - zP)^{-1}\mathbf{p}_0. \tag{23}$$

We keep both notations: $\tilde{F}$ for the CDF generating function and $\tilde{f}$ for the PMF generating function (used in AW inversion). The exact recursion in time domain is

$$f(t) = r^\top Q^{t-1}p_0, \quad t \geq 1, \tag{24}$$

so the generating function can be written as

$$\tilde{f}(z) = \sum_{t\geq 1} f(t)z^t = z\, r^\top (I - zQ)^{-1}p_0. \tag{25}$$

On the other hand, the renewal relation gives

$$\tilde{f}_{n_0 \to n_t}(z) = \frac{\tilde{P}_{n_0}(n_t, z)}{\tilde{P}_{n_t}(n_t, z)}, \tag{26}$$

which is equivalent: the former uses the transient submatrix Q, the latter uses the defect-free propagator. We then apply Abate–Whitt (AW) numerical inversion to extract coefficients:

$$f(t) \approx r^{-t} \frac{1}{m} \sum_{k=0}^{m-1} \tilde{f}(z_k)\, e^{-2\pi i k t/m}, \qquad z_k = r\, e^{2\pi i k/m}, \quad t = 1, \ldots, t_{\max}^{\mathrm{AW}}. \tag{27}$$

We choose $m = \mathrm{pow2}(\mathrm{oversample} \cdot (t_{\max}^{\mathrm{AW}} + 1))$ and set $r^m = 10^{-\text{r-pow10}}$, matching the repository defaults. Larger r reduces truncation error but increases numerical sensitivity; smaller r magnifies truncation error. We keep the auto-tuning strategy to balance stability and accuracy.

Implementation workflow (Algorithm box)

1. Build the spectral decomposition of the defect-free A (periodic/reflecting), yielding explicit mode sums for $\tilde{P}^e(n, z)$.
2. Construct $H(z)$ and vectors $\mathbf{a}, \mathbf{b}$ from the defect list, solve the linear system to obtain $\tilde{P}(n, z)$.
3. Use the renewal formula $\tilde{f}(z) = \tilde{P}_{n_0}(n_t, z)/\tilde{P}_{n_t}(n_t, z)$ to get the generating function.
4. Sample $z_k = re^{2\pi i k/m}$ and apply AW inversion to obtain $f(t)$.
5. Compare with exact recursion/MC, and record errors in the metrics JSON.

4 Numerical baseline: exact/flux recursion and MC

Exact recursion computes $f(t) = r^\top Q^{t-1} p_0$ (Eq. 24) as the deterministic baseline, and we overlay it with AW inversion and MC histograms (Fig. 7–24). MC trajectories are also classified into "fast/slow channels" to explain bimodality.

Peak and valley metrics For the smoothed $f(t)$, take the two dominant peak locations t_{p1}, t_{p2} and the minimum t_v between them, and define

$$h_1 = f(t_{p1}), \quad h_2 = f(t_{p2}), \quad \text{peak ratio} = \frac{\min(h_1, h_2)}{\max(h_1, h_2)}, \quad \text{valley ratio} = \frac{f(t_v)}{\min(h_1, h_2)}. \tag{28}$$

Note: For the scan in Fig. 1(b) we use

$$v_{\max} = \frac{h_v}{\max(h_1, h_2)},$$

while the main-text *valley ratio* is

$$v_{\min} = \frac{h_v}{\min(h_1, h_2)}.$$

The relation is

$$v_{\max} = v_{\min} \frac{\min(h_1, h_2)}{\max(h_1, h_2)} = v_{\min} \times \text{peak ratio}.$$

All figure annotations and configuration card values are produced by the same metrics pipeline and written to the metrics JSON to ensure consistency.

case	L^1 error	L^∞ error
A	1.56×10^{-13}	2.97×10^{-16}
B	5.04×10^{-13}	9.57×10^{-16}
C	1.10×10^{-13}	1.89×10^{-16}

Table 3: Errors between AW inversion and exact recursion for $t \leq t_{\max}^{\mathrm{AW}}$ (L^1 and L^∞).

5 Three constructions and mechanisms

We present the three candidates with construction details, mechanism interpretations, and numerical verification (figures are separated to avoid crowded panels).

5.1 Candidate A: periodic boundary + global bias

This follows the "periodic + bias" bimodality mechanism in PhysRevE 102, 062124. The fast channel is an against-drift shortcut; the slow channel is a with-drift wrap-around.

Configuration Card

- $N = 60$, $q = 0.8$, $g = (+0.6, 0)$, boundary: x periodic, y reflecting; start=(10,30), target=(12,30).
- Local structure: no local defects; bimodality comes purely from the wrap-around topology.
- Channel criterion: no x wrap-around is fast; at least one x wrap-around is slow (matches MC classification).
- Peak/valley metrics: $t_{p1} = 6$, $t_v = 110$, $t_{p2} = 232$; $h_2/h_1 = 0.374$; valley ratio$= 2.60 \times 10^{-5}$.

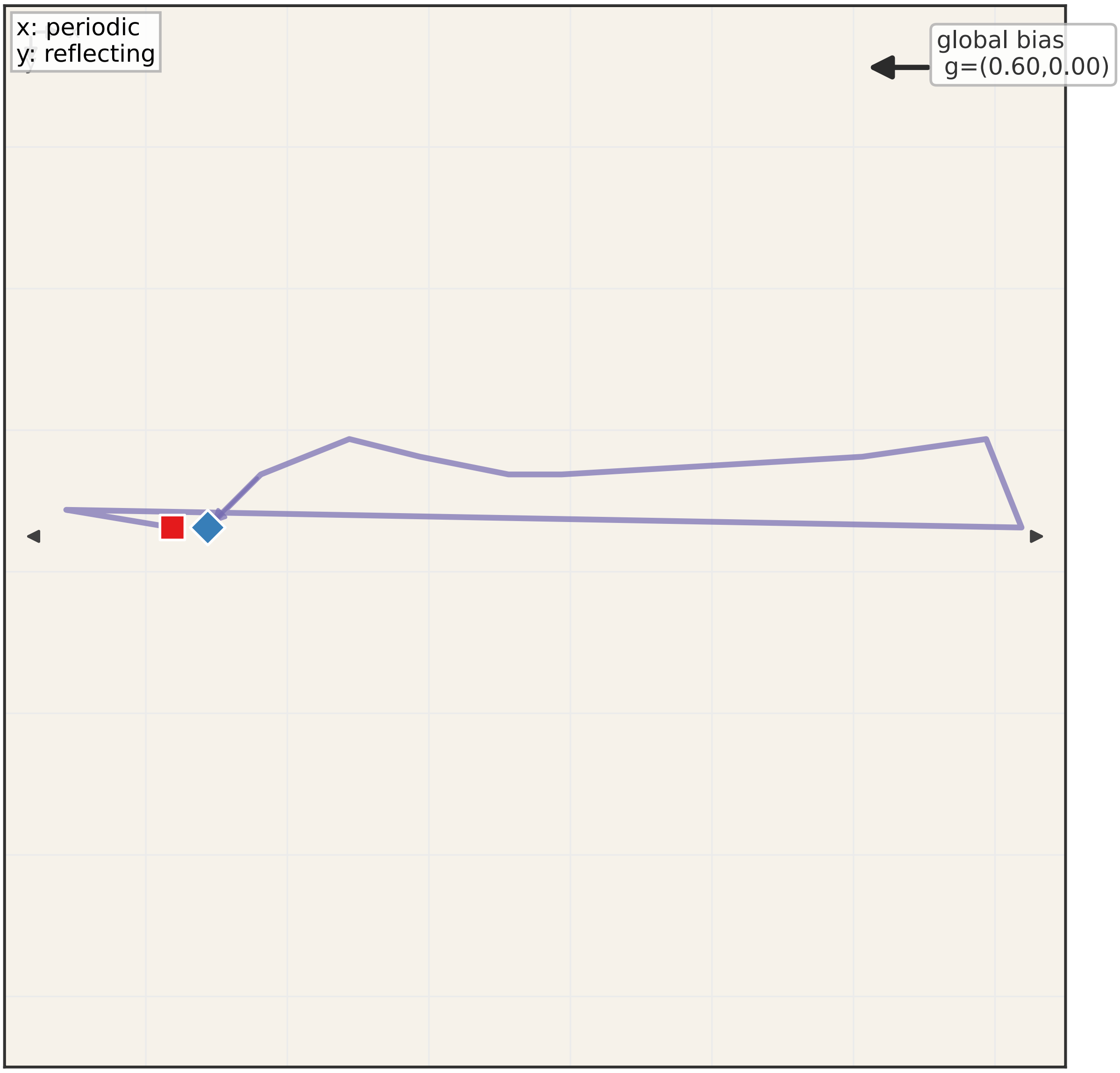

Figure 3: Candidate A: environment schematic. Symbols follow Fig. 2.

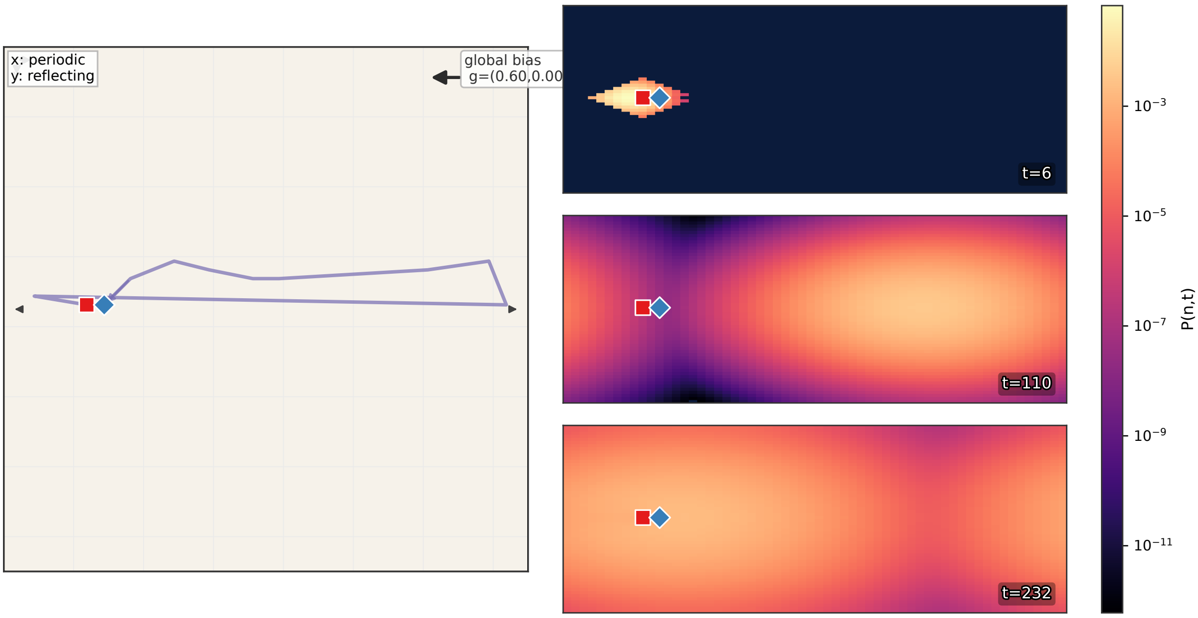

Figure 4: Candidate A: environment schematic and $P(n,t)$ slices at t_{p1}, t_v, t_{p2}.

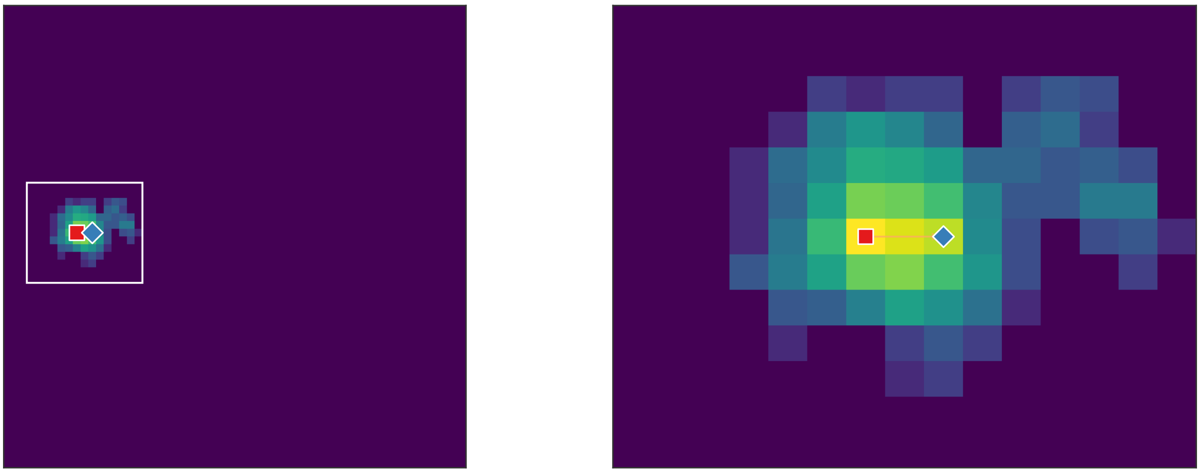

Figure 5: Candidate A: fast-channel trajectory density + representative paths (full + ROI).

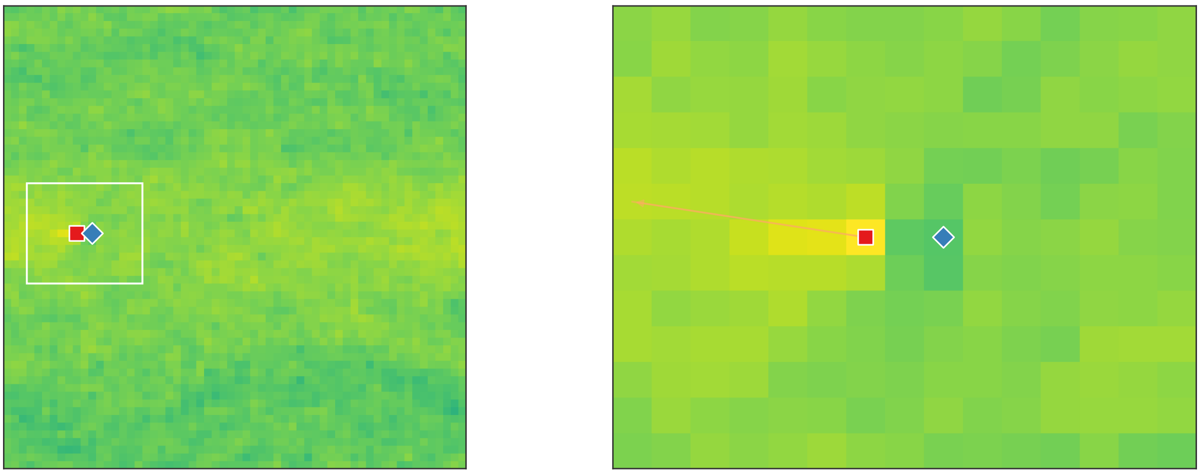

Figure 6: Candidate A: slow-channel trajectory density + representative paths (full + ROI).

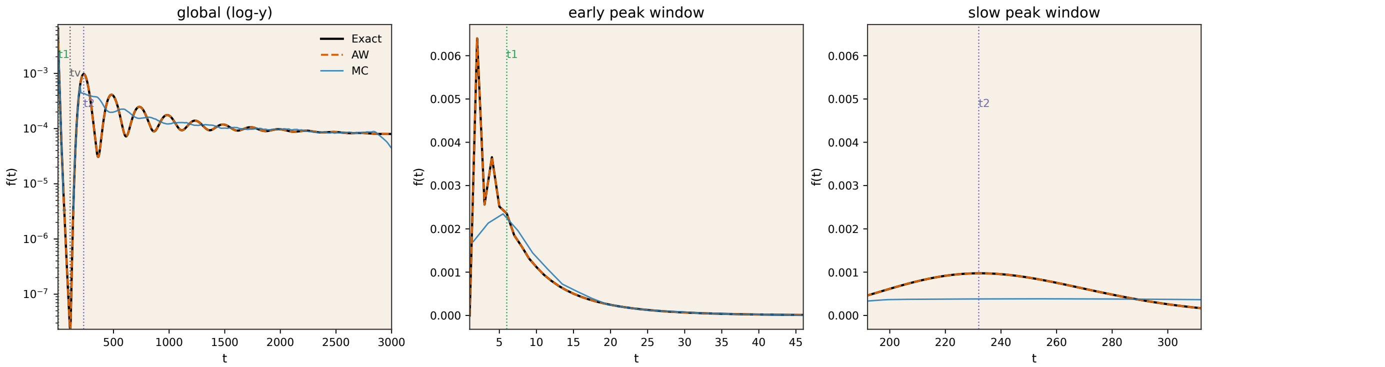

Figure 7: Candidate A: multiscale FPT plot (global log + fast/slow windows; Exact/AW/MC).

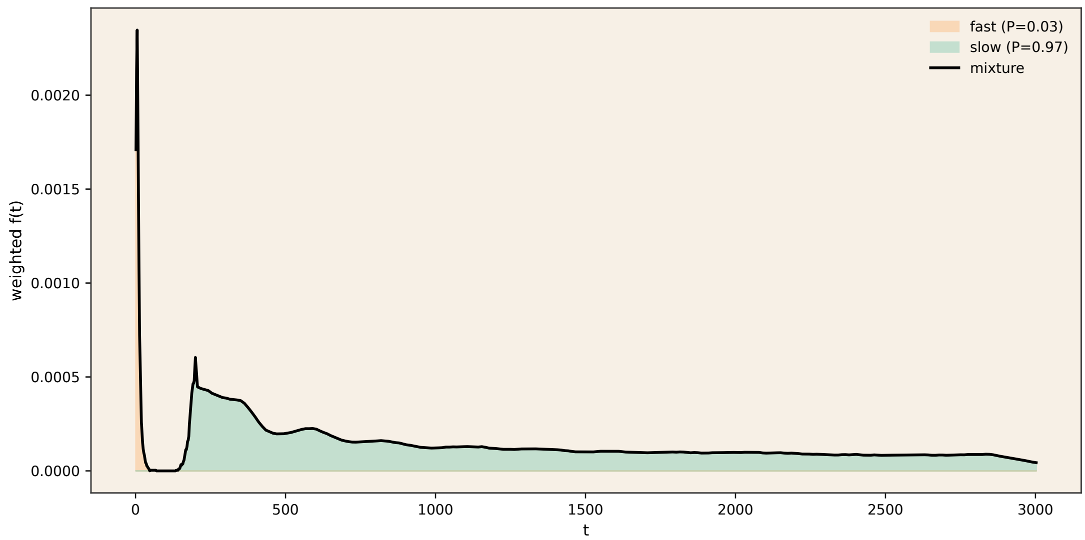

Figure 8: Candidate A: channel decomposition and mixture.

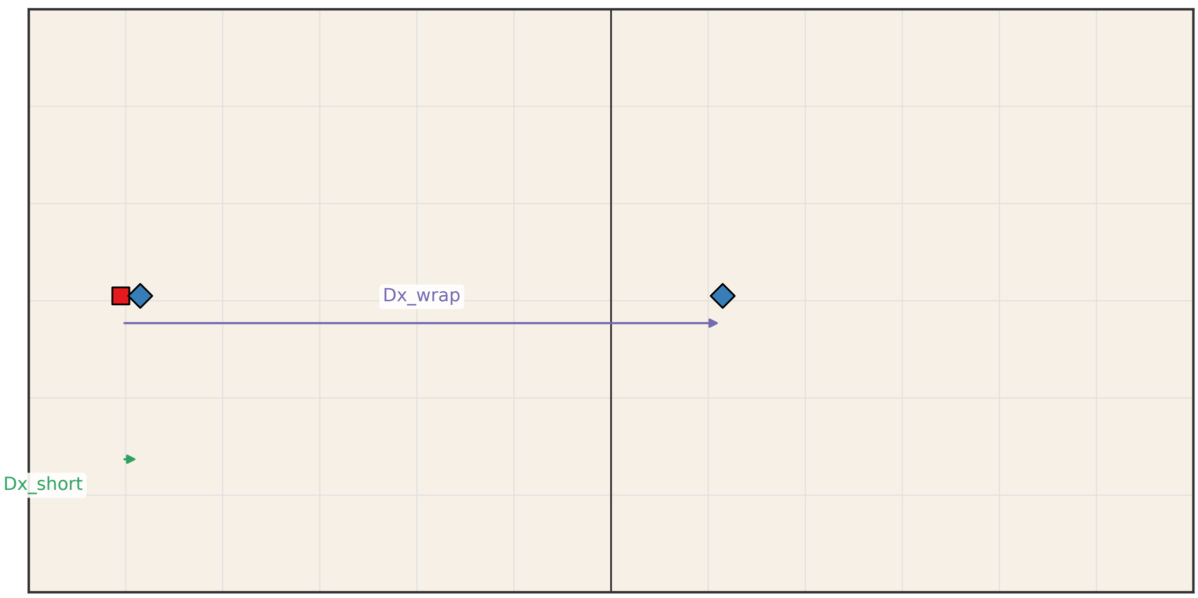

Figure 9: Candidate A: periodic unwrapped view (two tiles) with Dx_{short} and Dx_{wrap}.

5.2 Candidate B: edge corridor + mixed boundary

This study places the corridor on the reflecting edge ($y = N$) and enables auto-tuning of (g_x, g_y, δ) to meet the bimodality visibility threshold. If a pure reflecting boundary cannot satisfy the threshold, the tuner allows an x-periodic boundary to create a "wrap-around slow channel". Compared with an interior corridor, the edge corridor reduces escape and boosts the fast weight.

Failure baseline (interior corridor) A pure reflecting interior corridor yields too small a fast weight (the early peak becomes a shoulder), and is kept as a failure baseline to illustrate why "edge corridor + mixed boundary" is needed for visible bimodality.

Why is the interior-corridor early peak tiny? Why does an edge corridor fix it? The interior-corridor construction behaves as a "failure case": the corridor lies in an interior band, and escape in y occurs with probability $p_\uparrow + p_\downarrow \approx q/2$, so the probability of staying in the band for L steps is roughly $(1 - q/2)^L$. With $q = 0.8, L = 9$, this gives $(0.6)^9 \approx 1\%$, matching $P_{\text{fast}} \approx 0.01$ for that construction and making the early peak nearly invisible. The edge-corridor variant places the corridor on a reflecting boundary, so outward escape is reflected and only one-sided escape remains ($p_\uparrow \approx q(1 - g_y)/4$), raising the stay probability to $(1 - p_\uparrow)^L$, which can reach 10%–30%. This turns the early peak from "almost invisible" into "visibly bimodal"; the x-periodic boundary then provides a clear wrap-around time scale for the slow channel.

Configuration Card

- $N = 60$, $q = 0.8$, $g = (-0.25, +0.40)$, boundary: x periodic, y reflecting; start=(50,60), target=(42,60).
- Corridor: $y = 60$, $x \in [43, 50]$, direction left, $\delta = 0.70$, length $L = 8$; corridor band $y \in \{59, 60\}$.
- Channel criterion: stay in the corridor band until hitting the target is fast; leaving the band before hitting is slow (matches MC classification).
- Peak/valley metrics: $t_{p1} = 33$, $t_v = 220$, $t_{p2} = 473$; $h_2/h_1 = 0.989$; valley ratio= 6.04×10^{-2}.

Visualization tip The two peaks in Candidate B have a large height difference; semilogy + local windows are required to clearly see the early peak and valley (Fig. 15).

Bimodality detection and significance Fig. 16 runs peak detection (prominence + distance) on the smoothed curve, marks t_{p1}, t_{p2} and t_v, and reports the valley ratio; this filters out noisy shoulders and provides a consistent bimodality criterion.

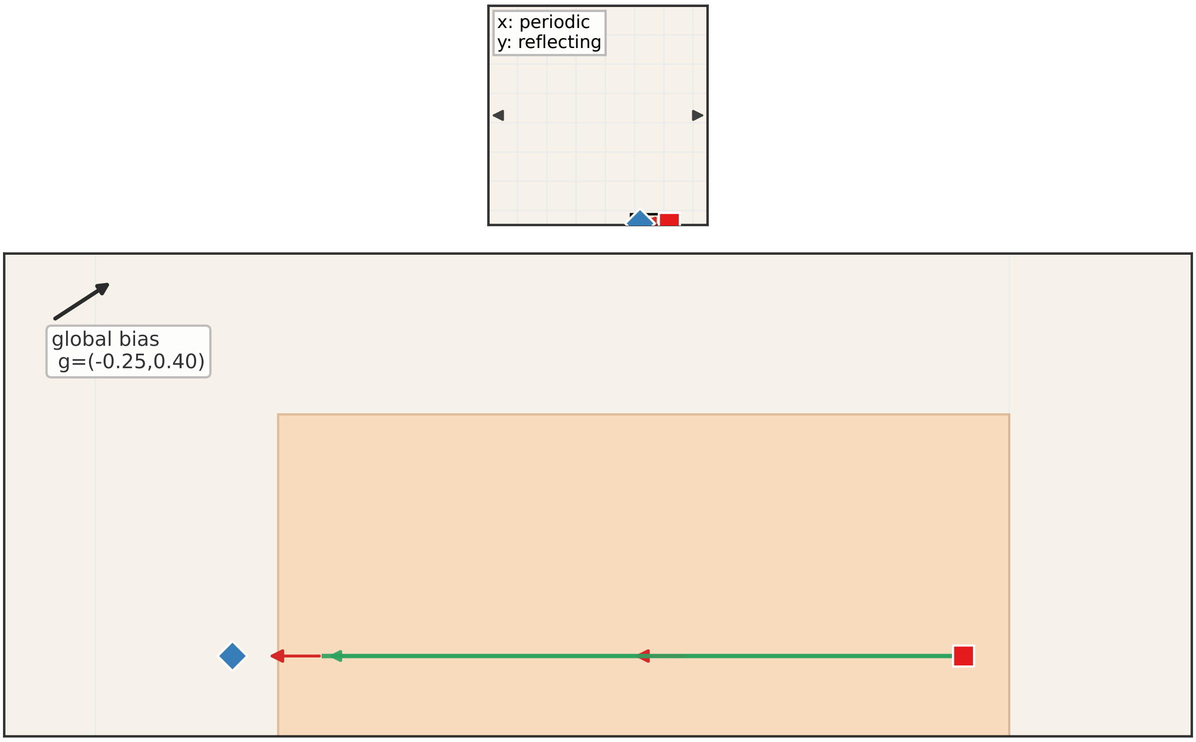

Figure 10: Candidate B: environment schematic (edge corridor + local bias).

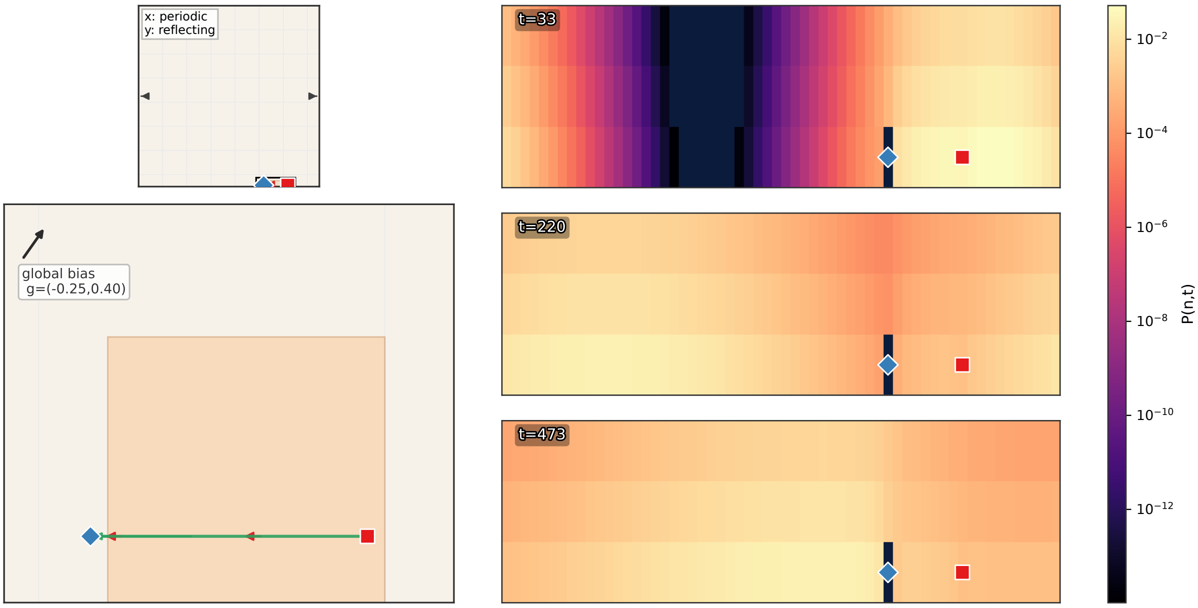

Figure 11: Candidate B: environment schematic and $P(n,t)$ slices at t_{p1}, t_v, t_{p2}.

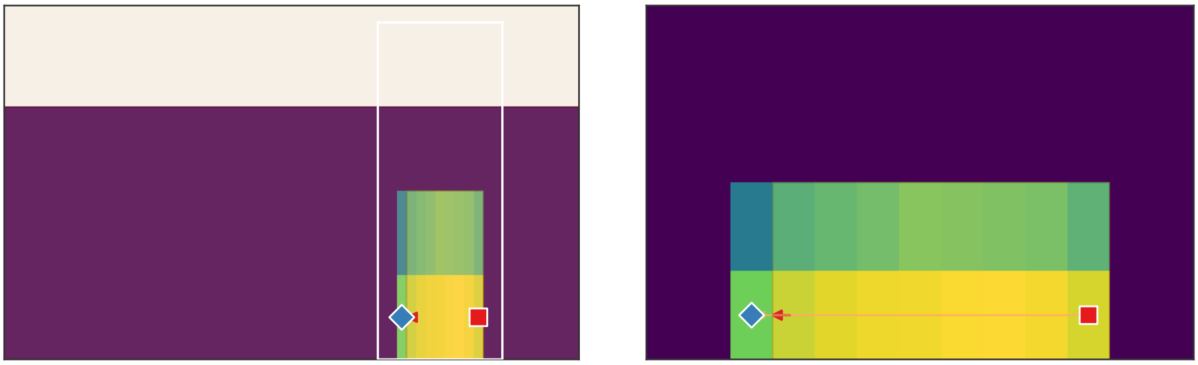

Figure 12: Candidate B: fast-channel density (corridor hits with small y fluctuations).

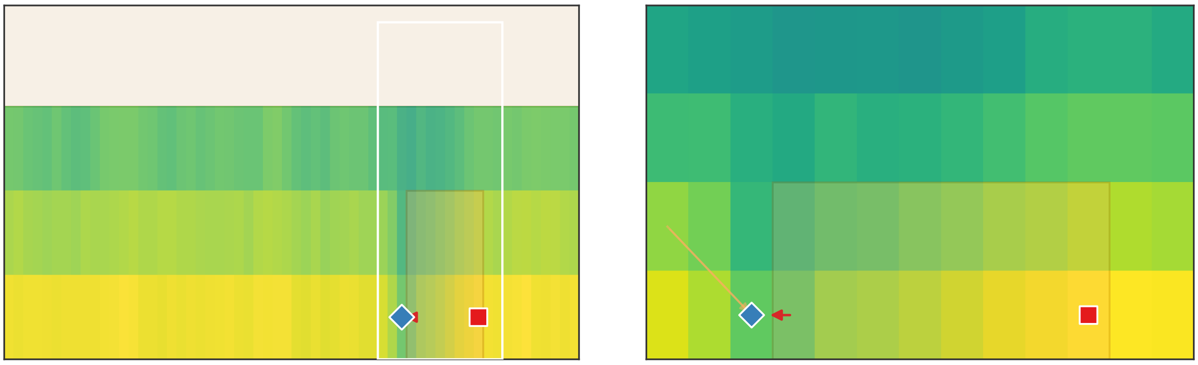

Figure 13: Candidate B: slow-channel density (wrap-around after leaving the corridor band).

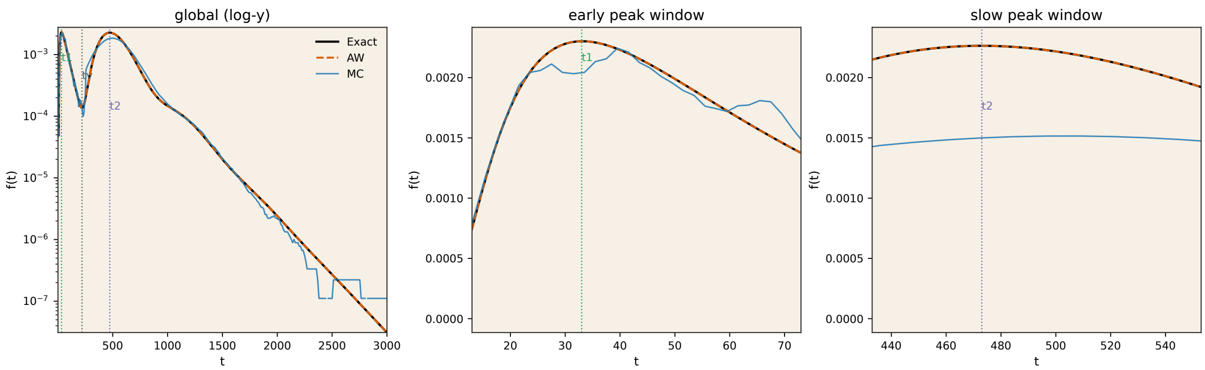

Figure 14: Candidate B: multiscale FPT plot (Exact/AW/MC).

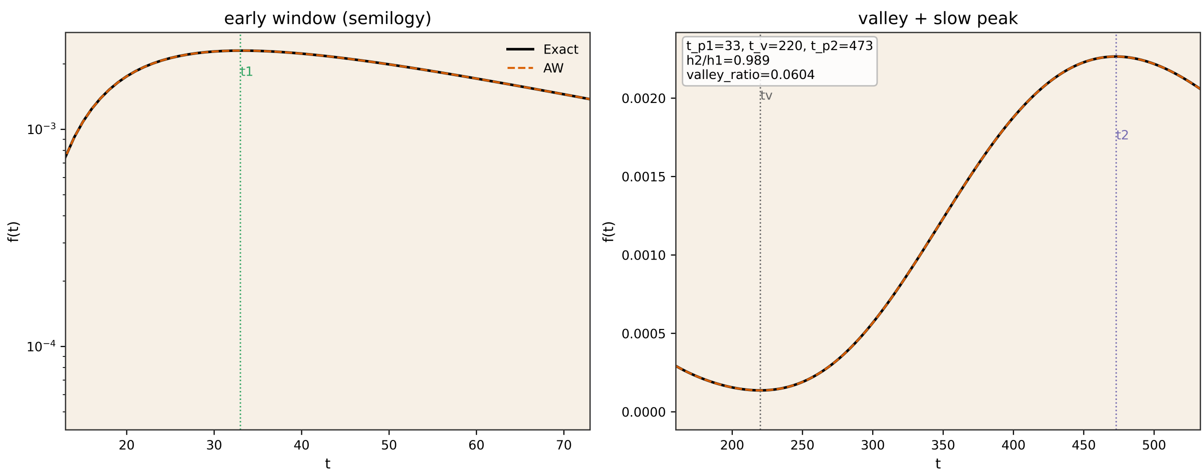

Figure 15: Candidate B: peak–valley zoom (semilogy + linear; t_{p1}, t_v, t_{p2} and valley ratio).

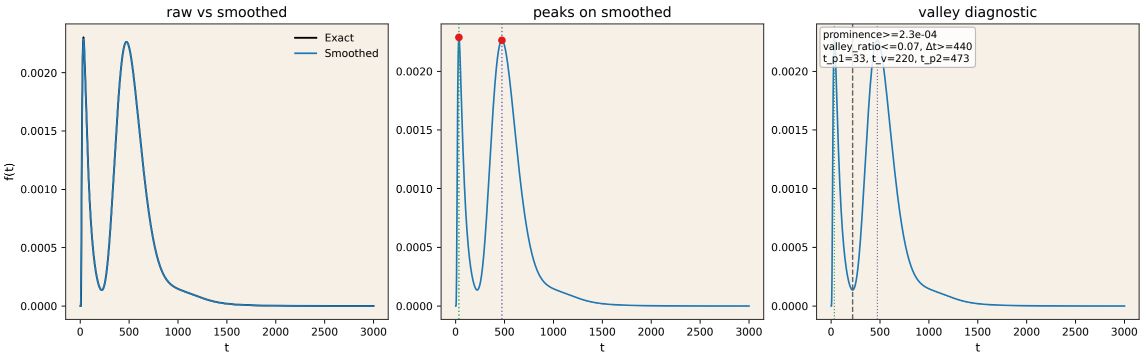

Figure 16: Candidate B: bimodality diagnostic (raw vs smoothed + peak finding + valley metrics).

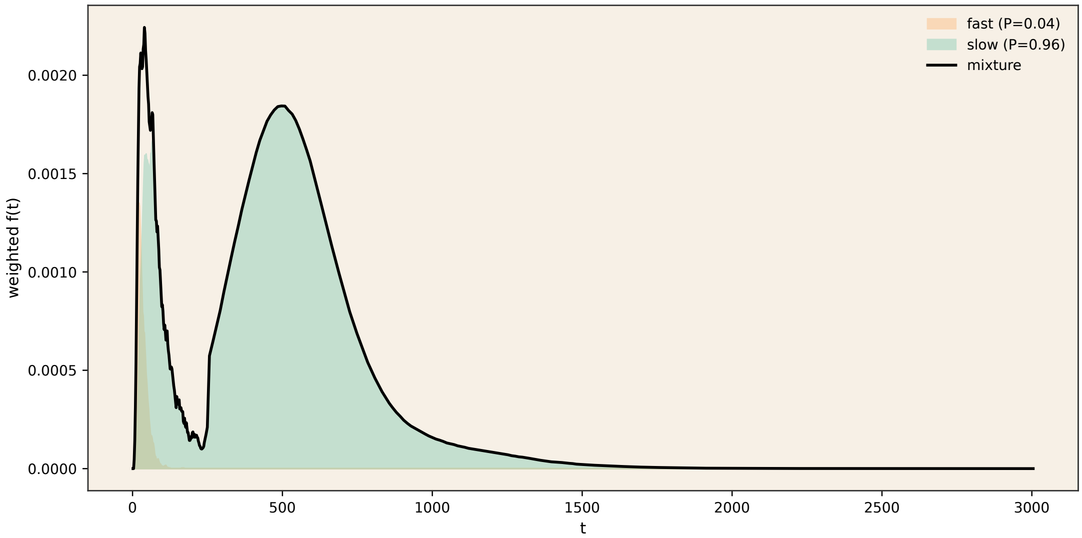

Figure 17: Candidate B: channel decomposition and mixture.

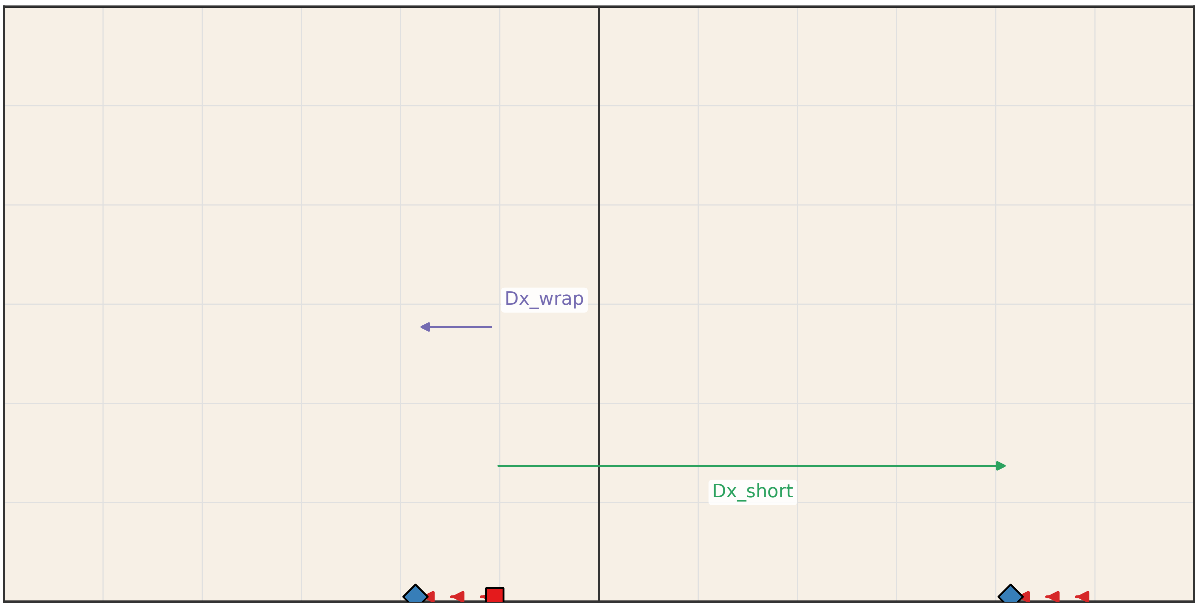

Figure 18: Candidate B: periodic unwrapped view (two tiles) showing the wrap-around slow channel.

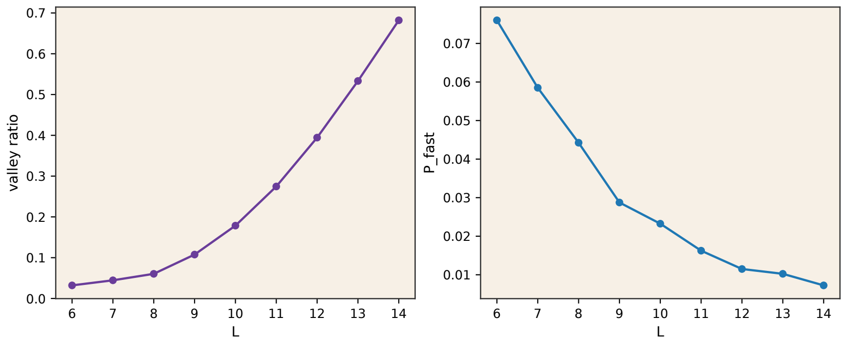

Figure 19: Candidate B: scan of L vs peak ratio and valley depth; $L_{\min} = 6$.

Failure case (interior corridor) With interior-corridor parameters, Candidate B has too small an early-peak weight ($P_{\text{fast}} \approx 1\%$), so the smoothed curve fails the bimodality criterion. This failure emphasizes that an edge corridor (higher stay-in-band probability) is essential for a visually and statistically clear bimodality.

5.3 Candidate C: door + sticky + wrap-around channel

We place a permeable door ($p_{\text{pass}} = 0.2$) on a vertical barrier and add a 3×3 sticky block (factor=0.2) to its left. With x-periodic boundary and leftward global bias ($g_x = +0.5$), we classify channels by first door-crossing time: early crossing is fast, late crossing (including wrap-around and sticky/door delays) is slow; bimodality already appears at $n_{\text{bias}} = 0$.

Configuration Card

- $N = 60$, $q = 0.8$, $g = (+0.5, 0)$, boundary: x periodic, y reflecting; start=(10,30), target=(50,30).
- barrier/door: a vertical wall at $x = 30$ reflects everywhere except a door at $(30, 30) \leftrightarrow (31, 30)$ with $p_{\text{pass}} = 0.2$.
- sticky: $x \in [27, 29]$, $y \in [29, 31]$, factor=0.2; number of local bias sites is 0.
- Channel criterion: first door-crossing time $\leq t_v$ is fast, otherwise slow.
- Peak/valley metrics: $t_{p1} = 88$, $t_v = 279$, $t_{p2} = 500$; $h_2/h_1 = 0.0326$; valley ratio= 2.19×10^{-2}.

Bimodality diagnostic Fig. 25 uses windowed two-peak selection with an early window [1, 200] and a late window [200, 1200] on the smoothed curve. It yields $t_{p1} = 88$, $t_v = 279$, $t_{p2} = 500$ and satisfies the unified criterion valley ratio ≤ 0.07.

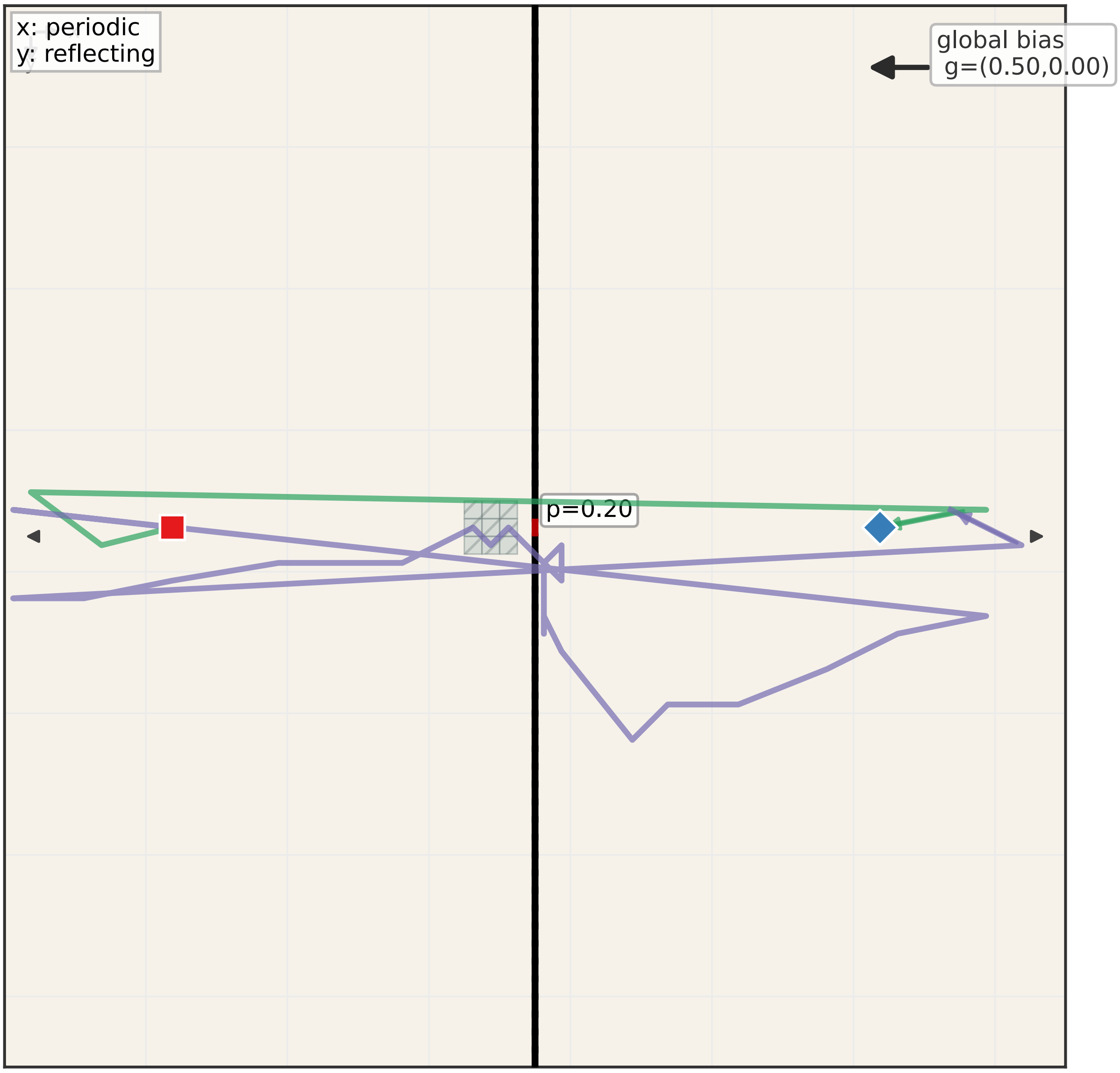

Figure 20: Candidate C: environment schematic (door/sticky highlighted).

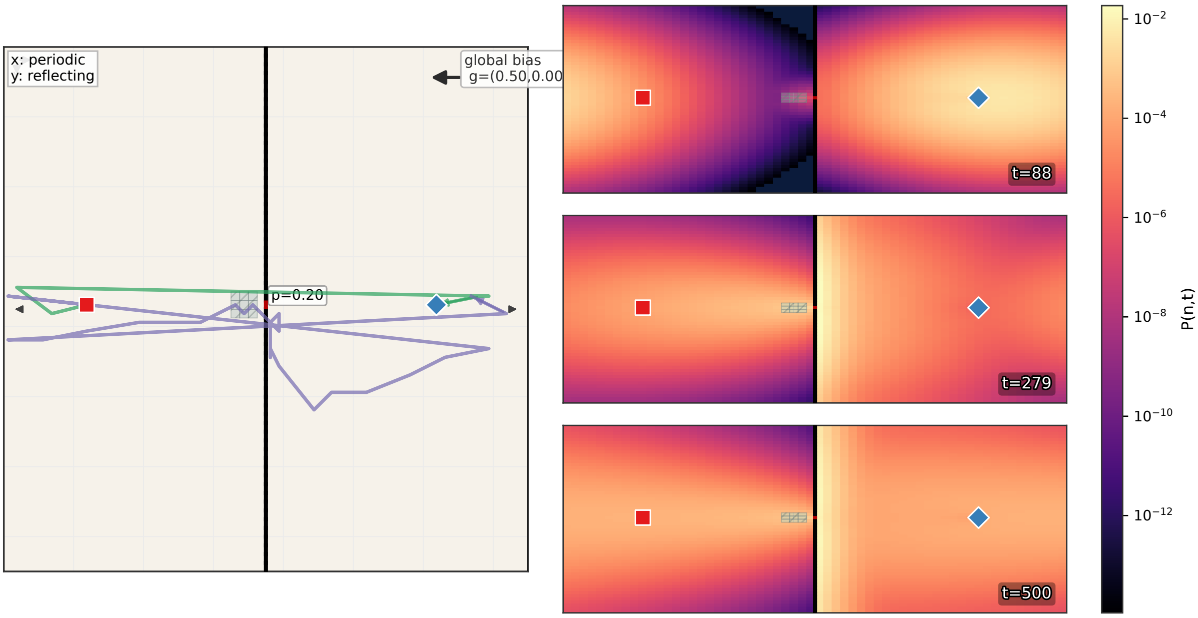

Figure 21: Candidate C: environment schematic and $P(n,t)$ slices at t_{p1}, t_v, t_{p2}.

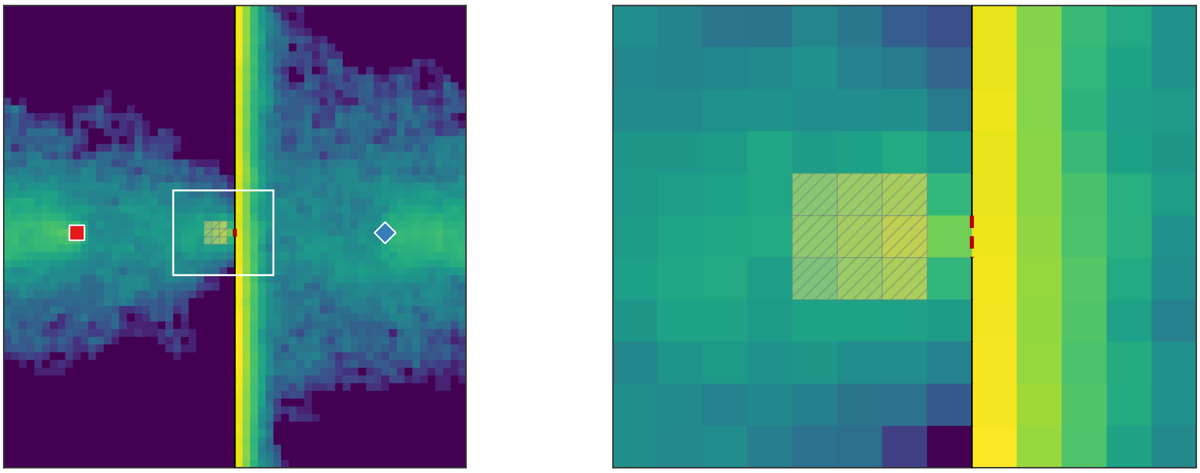

Figure 22: Candidate C: fast-channel density (early door crossing).

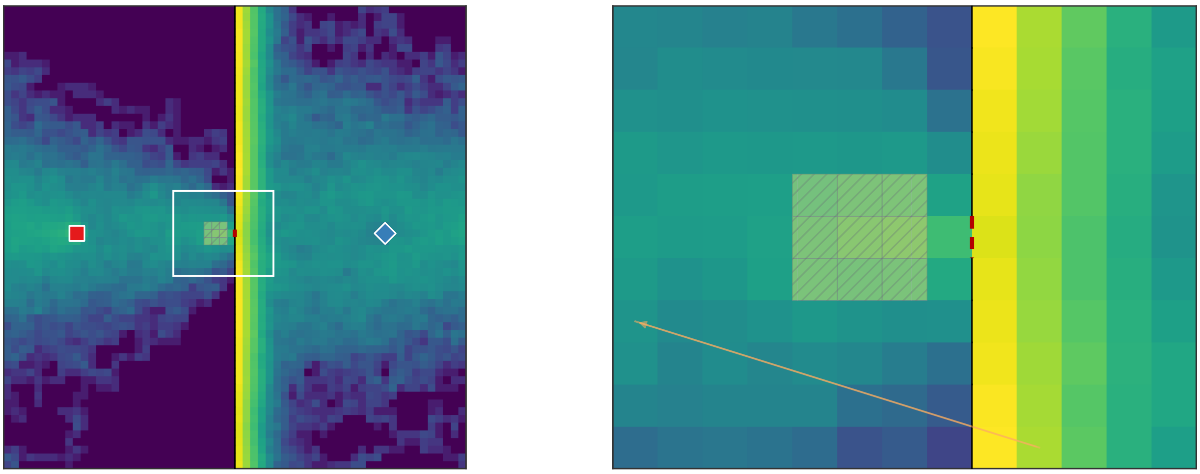

Figure 23: Candidate C: slow-channel density (wrap-around or sticky/door delays).

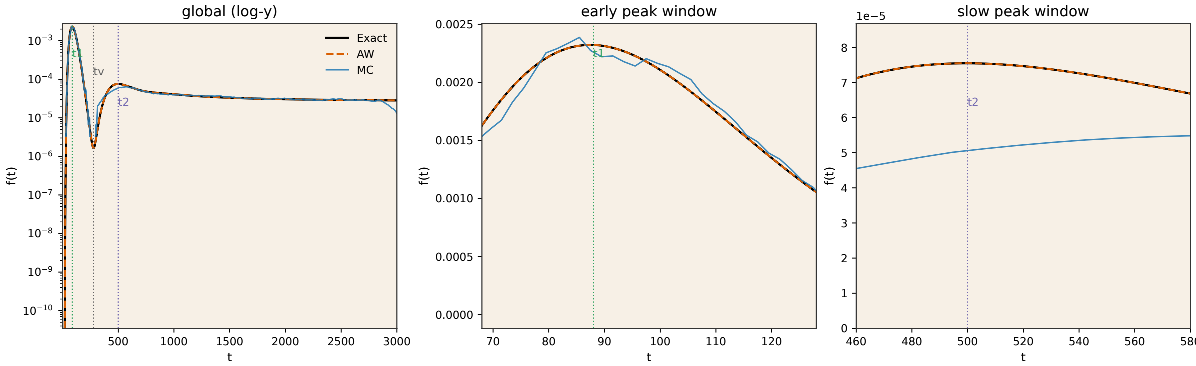

Figure 24: Candidate C: multiscale FPT plot (Exact/AW/MC, adaptive slow-window y-axis).

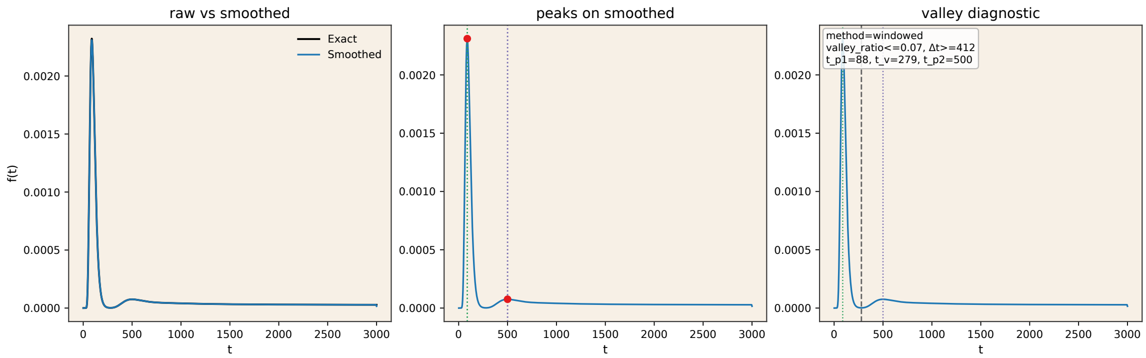

Figure 25: Candidate C: bimodality diagnostic (windowed two-peak; raw vs smoothed + peak finding + valley metrics).

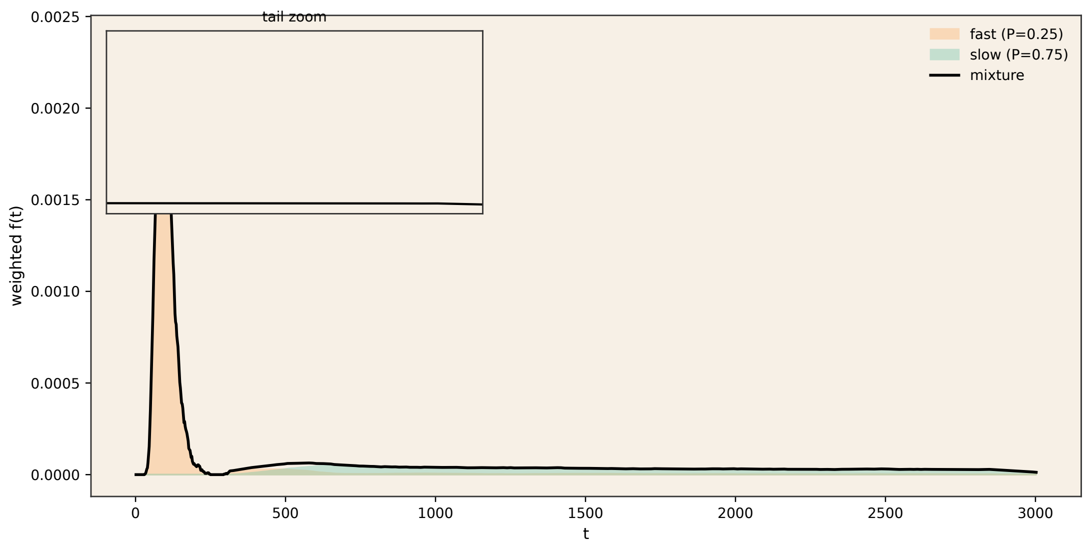

Figure 26: Candidate C: channel decomposition and mixture.

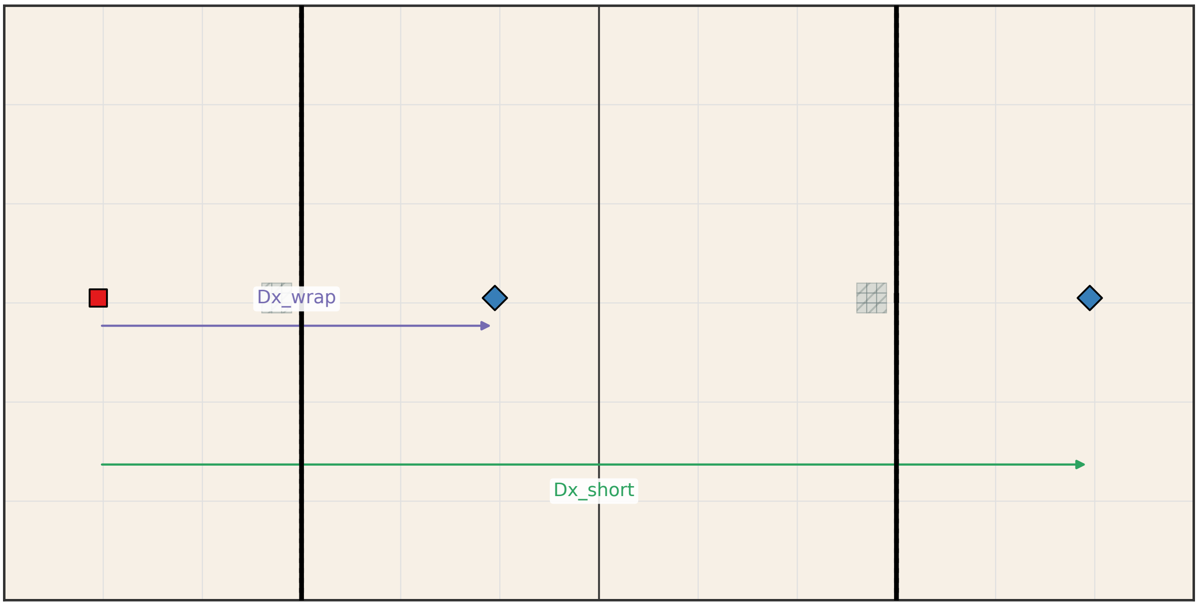

Figure 27: Candidate C: periodic unwrapped view (two tiles).

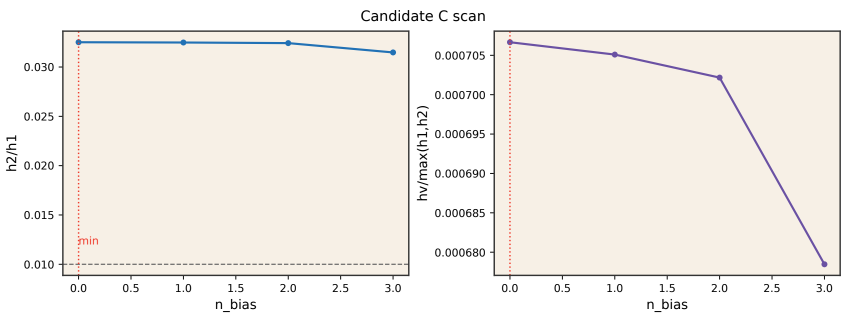

Figure 28: Candidate C: scan of local bias count; $n_{\min} = 0$.

6 Intuitive mechanism diagram: two-channel mixture + time-scale separation

Classify trajectories by channel event $C \in \{\text{fast}, \text{slow}\}$, then

$$f(t) = \mathbb{P}(C = \text{fast})\, f(t \mid C = \text{fast}) + \mathbb{P}(C = \text{slow})\, f(t \mid C = \text{slow}). \tag{29}$$

When the typical times satisfy $t_{\text{fast}} \ll t_{\text{slow}}$ and $\mathbb{P}(C = \text{fast})$ is not too small, a visible valley forms between the peaks.

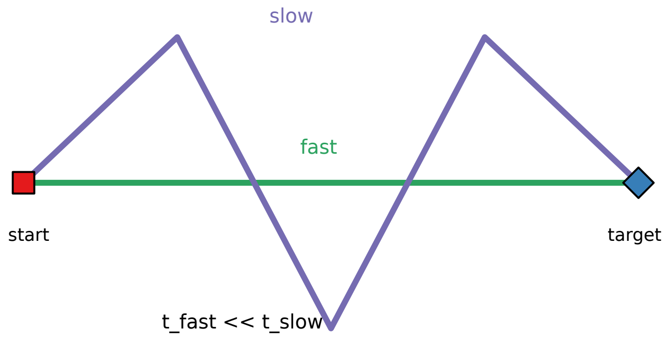

Figure 29: Conceptual cartoon: bimodality from two-channel mixture + time-scale separation.

Channel criteria (for fast/slow classification)

- A: whether x wrap-around occurs; no wrap is fast, any wrap is slow.
- B: whether the trajectory leaves the corridor band ($y \in \{59, 60\}$) before hitting; staying in the band is fast, leaving is slow.
- C: whether the first door-crossing time is later than t_v; early crossing is fast, late crossing is slow.

Geometric interpretation of the three candidates

- A: fast is an against-drift shortcut; slow is a with-drift wrap-around; periodic topology makes the slow channel natural.
- B: the edge corridor provides the fast channel; the x-periodic boundary plus global bias provides the wrap-around slow channel; scan yields $L_{\min} = 6$.
- C: door + sticky raise the cost of slow paths; early door crossing is fast, late door crossing with wrap-around or sticky delays is slow; the minimum local bias count is $n_{\min} = 0$.

Periodic unwrapped view The periodic mechanism for A, B, and C is shown in the unwrapped views (Fig. 9, Fig. 18, Fig. 27), with target images marked in two tiles and short vs wrap distances labeled as Dx_{short} and Dx_{wrap}.

Rough peak prediction The approximate drift speed is $v_x \approx q|g_x|/2$, giving a rough estimate $t_{\text{peak}} \approx \Delta x / v_x$. Table 4 compares the estimate with observed peak locations (for intuition only).

The prediction errors are larger for B/C because corridor bias, periodic wrap-around, and door/sticky delays modify the effective drift and waiting time. The table is for order-of-magnitude intuition only.

The shared mechanism can be summarized as follows:

- A: periodic topology provides a wrap-around slow channel; the against-bias shortcut yields the fast channel.

case	channel	Δx	t_{pred}	t_{peak}
A	fast (short)	2	8.3	6
A	slow (wrap)	58	241.7	232
B	fast (corridor)	8	80.0	33
B	slow (wrap)	52	520.0	473
C	fast (short)	20	100.0	88
C	slow (wrap)	40	200.0	500

Table 4: Rough peak predictions based on $v_x \approx q|g_x|/2$ vs observed peaks.

- B: the edge corridor provides the fast channel; the x-periodic boundary and global bias provide the wrap-around slow channel.
- C: door + sticky raise the door-crossing cost; early door crossing is fast, late crossing (including wrap-around or sticky/door delays) is slow.

7 Boundary conditions: physical meaning and rationale

reflecting Closest to diffusion/search in finite containers or walled domains: probability is conserved and does not "leak" out of the system.

periodic Corresponds to a ring/torus topology or a tiled homogeneous medium; less common in reality but naturally introduces a wrap-around slow channel (Candidate A).

mixed Periodic in one direction only (e.g., cylindrical surfaces or strip geometries), balancing realism and analytical control (Candidates B and C).

Recommendation If realistic boundaries are emphasized, consider a pure reflecting corridor baseline; if bimodality visibility is prioritized, use an edge corridor and allow an x-periodic boundary. If minimal local bias is a priority, Candidate A is simplest but more idealized; if one wants a controllable wrap-around mechanism within walled domains, Candidate C is more suitable.

8 Links to references

- PhysRevE 102, 062124: periodic boundary + bias yields bimodality (explicitly in 1D), matching Candidate A and the wrap-around channel in Candidate C.
- arXiv:2311.00464v2 Fig.3: construction rules for local bias, permeable barriers, and sticky sites (20% stay, 80/20 door, sticky factor 0.2), used in Candidates B/C.

9 Data and Code Availability

Scripts and data used in this study are organized under `reports/grid2d_bimodality/`. Figure outputs are stored in `figures/`, and numerical metrics and intermediate artifacts are stored in `data/` and `outputs/`. The PDF is compiled from the LaTeX source; running the main pipeline reproduces all figures and metrics following the same directory structure.

References

[1] S. Condamin et al., *Phys. Rev. E* **102**, 062124 (2020).

[2] M. Abad et al., *arXiv:2311.00464v2* (2023).